Large eddy simulations of a buoyant plume above a heated horizontal cylinder at intermediate Rayleigh numbers

Stig Grafsrønningen[a], Atle Jensen[a,1,*]

[a]*Mechanics Section, Department of Mathematics, University of Oslo (UiO), P.O. Box 1053, Blindern, NO-0316 Oslo, Norway*

Abstract

Large eddy simulations of a buoyant plume forming above a heated horizontal cylinder with a Rayleigh number of 9.4E7 is carried out and compared with experimental data. Natural convection heat transfer from a horizontal cylinder at this intermediate Rayleigh number involve a laminar to turbulent transition downstream the cylinder. A laminar to turbulent transition will alter the flow characteristic downstream cylinder considerably, thus it is important that the transition is captured in the simulations. Subgrid stresses are accounted for using the dynamic Smagorinsky model which allow for both laminar and turbulent flow through the dynamic procedure.

The results show a considerable difference between the numerical and experimental results. Plume center vertical velocity is highly overpredicted compared to the experimental data. The computed half-width about 1.5 y/D downstream the cylinder is comparable to the experimental data, however, 3.5 y/D downstream cylinder, the half-width is only about half that of the experimental data. The half-width growth rate measured in the experiments remain higher than the computed growth rate throughout the domain of interest.

Keywords: turbulent plumes, natural convection, horizontal cylinder, LES,

*Corresponding author

[1]Email: atlej@math.uio.no, Telephone: +47 924 62282

transition

Nomenclature

C_p	Specific heat capacity $-$ (J/kgK)
D	Cylinder diameter $-$ (m)
Gr	Grashof number $-$ $\frac{g\beta(T_w - T_\infty)D^3}{\nu^2}$ $(-)$
$Gr_{Q,Y}$	Local Grashof number $\frac{g\beta Q y^3}{\rho C_p \nu^3}$ $(-)$
Nu	Nusselt number $-$ $\frac{hD}{k}$ $(-)$
P	Pressure $-$ (Pa)
Pr	Prandtl number $-$ $\frac{\nu}{\alpha}$ $(-)$
Q	Heat per length $-$ (W/m)
R	Cylinder radius $-$ (m)
Ra	Rayleigh number $-$ $\frac{g\beta(T_w - T_\infty)D^3}{\alpha\nu}$ $(-)$
T	Temperature $-$ (K)
U	Horizontal velocity $-$ (m/s)
V	Vertical velocity $-$ (m/s)
W	Spanwise velocity $-$ (m/s)
g	Gravity $-$ (m/s^2)
k	Thermal conductivity $-$ (W/mK)
t	Temperature fluctuation $-$ (K)
u	Horizontal velocity fluctuation $-$ (m/s)
v	Vertical velocity fluctuation $-$ (m/s)

w	Spanwise velocity fluctuation $-$ (m/s)
x	Cartesian coordinate, horizontal distance from cylinder center $-$ (m)
y	Cartesian coordinate, vertical distance above cylinder center $-$ (m)

Greek

α	Thermal diffusivity $-$ $\frac{k}{\rho C_p}$ (m^2/s)
β	Coefficient of thermal expansion $-$ $(1/K)$
η	Length scale $-$ (m)
μ	Molecular viscosity $-$ (kg/ms)
ν	Kinematic viscosity $-$ (m^2/s)
ρ	Density $-$ (kg/m^3)
θ	Circumferential angle $-$ $(^\circ)$
ϑ	Dimensionless coordinate $-$ $\frac{x}{y-B}$ $(-)$

Subscripts

∞	Ambient condition
B	Batchelor
f	Film condition evaluated at $(T_w + T_\infty)/2$
$Inf.$	Inflection point
w	Wall condition

Superscripts

$-$	Ensemble average
$\sim$	Filtered quantity

List of Figures

b).

Fig. 10: Volume flux per unit length $F = \int V(x)dx$ above cylinder for – LES and $--$ experiments, corrected for draft velocity.

Fig. 11: Sum of mean kinetic energy $\sum K = \int 0.5(\bar{U}^2 + \bar{V}^2)dx$ and estimate for fluctuating kinetic energy $\sum k = \int 0.5(\overline{u^2} + \overline{v^2})dx$ across plume. Upper lines show $\sum K$ whereas lower lines show $\sum k$ for – LES and $--$ experiments.

Fig. 12: a) Plume center vertical velocity $\bar{V}$ and b) plume center temperature excess $\Delta\bar{T}$. The dotted line is theoretical (fitted) temperature decay $T \sim 1/y$.

Fig. 13: a) LES b) experiments – Vertical velocity V and horizontal velocity U, $\bullet$ 90 mm, $*$ 110mm, $\triangle$ 130mm, $\bigcirc$ 150 mm, $\square$ 170 mm, and $\star$ 190 mm above pipe center.

Fig. 14: Volume visualization of temperature, velocity and pressure. 1s apart, left to right. See http://tinyurl.com/cxsntun for movie.

Fig. 15: Instantaneous horizontal velocity $\tilde{U}$ in yz-plane above cylinder.

1. Introduction

Natural convection heat transfer from horizontal cylinders have been under scrutiny for about a century, see e.g. Grafsrønningen et al. [2] for a brief summary of the earliest papers. Research on natural convection heat transfer from horizontal cylinders has resurfaced a number of times since the first theoretical and experimental investigations with the introduction of new experimental, analytical or numerical techniques, and a vast number of articles have been published within the topic. Natural convection heat transfer from horizontal cylinders has a fundamental significance in design of heat exchangers, pipelines, HVAC-systems and other applications. In buoyant flows the Nusselt number Nu, Rayleigh number Ra, Grashof number Gr and Prandtl Pr number play vital roles. The Nusselt number is a measure of the ratio between convective to conductive heat transfer from solids to fluids, whereas the Rayleigh number is the product of the Grashof number and Prandtl number $Ra = GrPr$. The Grashof number is the ratio of buoyant forces and viscous forces and the Prandtl number Pr is kinematic viscosity over thermal diffusivity. A number of empirical correlations which relates the Nusselt number to the Rayleigh number exists, cf. Morgan [3] or Kitamura et al. [4]. However, in design of complex heat exchangers based solely on natural convection heat transfer, empirical correlations for a single unbounded horizontal cylinder under quiescent conditions are not sufficient. The correlations would not yield satisfactory results, cf. e.g. Gyles et al. [5].

Computational Fluid Dynamics (CFD) is widely used in design of heat exchangers. CFD is an excellent tool, when used correctly, which may provide results for complex geometries in a fraction of the time it takes to build an experimental setup and at significantly reduced cost. When used together and verified against experiments, CFD may provide knowledge about unmeasurable

quantities, or yield results about small scale features which hardly are measurable.

Design of subsea heat exchangers based solely upon natural convection heat transfer, with the aid of CFD tools, is not straightforward. Natural convection flow associated with full scale heat exchangers for the energy sector are often turbulent, or undergoing a laminar to turbulent transition. The CFD tools must therefore be able to predict the onset of transition from laminar to turbulent flow accurately without any knowledge of the route to turbulent flow nor tuning of turbulence models. This is most likely the single most important physical feature the simulation must capture which makes heat transfer predictions especially challenging.

Subsea heat exchangers are vital parts of subsea gas boosting modules and other subsea processing modules. A subsea heat exchanger may consist of multiple connected horizontal cylinders forming meandering tubes, see Gyles et al. [5] for an example. Grafsrønningen et al. [2] and Grafsrønningen and Jensen [1] investigated the buoyant plume forming above a single heated horizontal cylinder in a quiescent environment. The results showed that the plume transitioned from laminar to turbulent flow a distance downstream the cylinder.

Pham et al. [6] pointed out that pure thermal plumes are examples of very complex flows due to quick unstable growth resulting in abrupt transition from laminar to turbulent flow. Thus despite its very simple geometry, the buoyant plume forming above a single cylinder involves a troublesome laminar to turbulent transition, hence simulations of a single heated horizontal cylinder and comparison with experimental results may provide valuable feedback on the performance of CFD-tools for such applications. A transition will influence the transport and mixing properties downstream the cylinder significantly and possibly influence the efficiency and design of large heat exchangers to a

great extent. It is therefore important that the transition is captured in the simulations.

Contradictory to pipe flow, where large perturbations are required to trigger turbulent flow, linear stability theory show that buoyant plumes are unstable to infinitesimal perturbations, thus a reproducible transition onset should be obtainable in numerical simulations, cf. Eckhardt [7] and Gebhart et al. [8]. Downstream a critical location, which is available from linear stability theory and some critical local Grashof number, the flow is unstable to ever-present minute disturbances.

Natural convection heat transfer from heated horizontal cylinders has been investigated by a number of researchers. Kuehn and Goldstein [9] studied laminar natural convection heat transfer from a horizontal cylinder numerically for Rayleigh number ranging from 1 to $1E7$. Farouk and Güçeri [10] investigated laminar natural convection heat transfer from a horizontal cylinder using a finite difference technique. Merkin and Pop [11] examined natural convection heat transfer around and above a cylinder by solving a set of boundary layer equations. Saitoh et al. [12] presented results from numerical simulations of laminar natural convection flow around a heated horizontal cylinder as a benchmark solution for various Rayleigh and Prandtl numbers. Yüncü and Batta [13] investigated laminar natural convection heat transfer from a single and two vertically arranged horizontal cylinders using a finite difference technique. Recently Demir [14] investigated laminar natural convection heat transfer from a concrete cylinder numerically.

The articles mentioned hitherto were all of laminar natural convection heat transfer, i.e. turbulent effects were either not present or neglected. Even though the Rayleigh number based on the cylinder diameter implies laminar flow, the plume often undergoes a transition to turbulent flow downstream the cylinder.

Noto et al. [15] investigated the buoyant plume forming above a horizontal wire in air. The Rayleigh number based on wire diameter was in the order of unity, yet the plume underwent a transition from laminar to turbulent flow downstream the cylinder. Noto et al. [15] presented a transition criteria for planar buoyant plumes above cylinders or wires based on the local Grashof number $Gr_{Q,Y} = \frac{g\beta QY^3}{\rho C_p \nu^2}$. If $Gr_{Q,Y}$ is less than $2E8$ the flow is laminar, if $2E8 < Gr_{Q,Y} < 2E9$ the flow is transitional, and for $Gr_{Q,Y} > 2E9$ the flow is turbulent. Hence, turbulent effects cannot be neglected in plumes, particularly not downstream the cylinder were accurate predictions of the flow and temperature fields are required. The criterion proposed by Noto et al. [15] was compared with the experimental results by Grafsrønningen et al. [2] and Grafsrønningen and Jensen [1] and showed a relatively good fit.

Farouk and Güçeri [16] used a $k-\varepsilon$ model to account for turbulent effects and computed the natural convective flow around a cylinder at Rayleigh numbers ranging from $Ra = 5E7$ to $1E10$. However, as pointed out by Kitamura et al. [4], the flow around the lower part ($\theta < 120°$) of a horizontal cylinder will still be laminar even for large Rayleigh numbers ($Ra \gtrsim 1E11$). Thus the flow around a single cylinder involves a laminar to turbulent transition which is hardly tractable by RANS-models.

Bastiaans et al. [17] carried out Direct Numerical Simulations (DNS) and Large Eddy Simulations (LES) of a transitional planar plume forming above a horizontal heated wire in air in an enclosed cavity, where they investigated the performance of several LES subgrid models.

Many articles on LES/DNS of turbulent buoyant plumes exist in the literature. However, the bulk is on buoyant plumes from jets or other similar momentum carrying sources. Moreover, turbulent simulations, i.e. LES or DNS, of natural convection heat transfer from unconfined heated horizontal cylinders

have, to the authors knowledge, not been carried out before. Thus the authors have recognized the need for accurate turbulent simulations of an unconfined horizontal cylinder with comparison against detailed experimental results.

2. LES

LES simulations were carried out using CDP; a multipurpose, unstructured finite-volume based LES code developed at Center for Turbulence Research at Stanford University's Centre for Integrated Turbulence Simulations, cf. e.g. Ham et al. [18], Ham and Iaccarino [19], Ham et al. [20], and Pierce [21].

The equations solved are the filtered continuity equation

$$\frac{\partial \tilde{U}_k}{\partial x_k} = 0, \tag{1}$$

and the filtered incompressible Navier-Stokes equations with a body force term to account for buoyant forces.

$$\frac{\partial \tilde{U}_i}{\partial t} + \tilde{U}_k \frac{\partial \tilde{U}_i}{\partial x_k} = -\frac{1}{\rho_0}\frac{\partial \tilde{P}}{\partial x_i} + \frac{\partial}{\partial x_k}(\nu \frac{\partial \tilde{U}_i}{\partial x_k}) - \frac{\partial \tau_{ij}}{\partial x_j} + g_i \beta \Delta \tilde{T} \tag{2}$$

Additionally a filtered scalar equation for the temperature field $\tilde{T}$ must be solved.

$$\frac{\partial \tilde{T}}{\partial t} + \tilde{U}_k \frac{\partial \tilde{T}}{\partial x_k} = \frac{\partial}{\partial x_k}(\alpha \frac{\partial \tilde{T}}{\partial x_k}) - \frac{\partial q_k}{\partial x_k} \tag{3}$$

The subgrid-scale stress term tensor $\tau_{ij} = \widetilde{u_i u_j} - \tilde{u}_i \tilde{u}_j$ is modeled using the dynamic procedure, see e.g. Germano et al. [22]. The dynamic Smagorinsky model was introduced to overcome the problem with varying model coefficients in inhomogeneous flows and close to solid boundaries cf. e.g. Pope [23]. For more details regarding implementation of this model in CDP, see the Appendix in Rashid et al. [24]. Furthermore, the definition of functions are to be found in Pope [23]. Thus the subgrid-scale stresses obtained from the dynamic Smagorin-

sky model vanish in laminar flow and at solid boundaries, see Germano et al. [22], or if the computational grid is sufficiently fine for the simulation to be a direct numerical simulation. Particularly in transient buoyant plumes the original Smagorinsky model does not emulate the turbulent stresses and requires extensive tuning of the model constants, cf. Webb and Mansour [25]. Worthy [26] compared a number of different turbulence models on a buoyant plume induced by a jet and concluded that the dynamic models performed unquestionably better than their static counterparts. The subgrid stresses are accounted for in the filtered Navier-Stokes equations using $\tau_{ij} - 1/3\tau_{kk}\delta_{ij} = -2\nu_t\tilde{S}_{ij}$ where ν_t denotes the turbulent viscosity. Similarly the subgrid fluxes $q_i = \widetilde{u_i t} - \tilde{u}_i\tilde{t}$ are accounted for in the filtered energy equation through $q_i = \alpha_t \frac{\partial T}{\partial x_i}$ where α_t is turbulent diffusivity.

The eddy viscosity ν_t and the eddy diffusivity α_t are here assumed to be related through a turbulent Prandtl number $Pr_t = \nu_t/\alpha_t = 0.9$. As pointed out by Pham [6] and others, the turbulent Prandtl number is generally not known and may vary between applications. You and Moin [27] calculated the turbulent Prandtl in turbulent channel flow. Their results showed that $Pr_t \simeq 1$ close to the wall. Bastiaans et al. [17] reported that values of 1/3 to 1/2 are common whereas Worthy [28] used values of 0.4 for Pr_t in LES of turbulent jets. Yan [29] carried out LES of turbulent thermal plumes and investigated the effect of turbulent Prandtl number Pr_t, and reported that the turbulent Prandtl number had little influence on the results. The turbulent Prandtl number is a flow property, and not a material property, thus it has no relation with the molecular Prandtl number Pr.

Bastiaans et al. [17] pointed out that there are regions with reversed energy transfer, so-called "backscatter", in a plume. There is not only inter-scale kinetic energy transfer from large to small scales, but also a nonlinear transfer

of energy from small to large scales which is of imperative importance. Within the framework of the eddy viscosity concept, the reversed energy transfer would correspond to $\nu_t < 0$ which numerically is destabilizing. To avoid negative viscosities and subsequently instability issues, clipping was employed by Bastiaans et al. [17]. CDP allows for negative turbulent viscosities, hence energy interchangeability between small and large scales is possible. However, to avoid numerical instabilities, the effective viscosity was clipped to allow only small negative values, i.e. $\nu_t \geq -\nu$. Moreover, to predict the transitional onset accurately, a fine mesh in the transitional region is required. Clipping of the turbulent viscosity may lead to incorrect results, thus it is important that the mesh is fine enough so clipping is avoided. An assessment of the negative part of ν_t in the transitional region showed that $|\nu_t/\nu|$ was significantly smaller than unity, i.e. negative turbulent viscosities was not bounded by $\nu_t \geq -\nu$, thus backscatter is not prevented by clipping.

When large temperature differences are present, the physical characteristics of the fluid may change. Here, the working fluid is water and the local change in material properties due to temperature differences within the temperature range are not negligible. The molecular viscosity μ in particular is highly temperature dependent. Furthermore, the thermal conductivity k and the coefficient of thermal expansion β change considerably with temperature and are treated accordingly.

Generally, as pointed out by Ferziger and Perić [30], the coupling between the energy and momentum equations generally is weak, and the solution may be solved sequentially. However, in buoyant flows, the only source of energy is $g_i\beta\Delta T$ where the temperature excess is denoted by ΔT. Hence, the coupling between the momentum and energy equations is strong. Furthermore, the dynamic behavior of turbulent kinetic energy depends directly on the heat

flux which constitutes a significant indirect coupling between the thermal and momentum fields. An accurate prediction of turbulent kinetic thus requires an accurate prediction of the correlation between the fluctuating temperature and velocity fields.

CDP uses a fractional-step method to advance in time, cf. e.g. Kim and Moin [31], Mahesh et al. [32] or Ferziger and Perić [30]. For each time step an inner loop is cycled through, the dependent variables are solved successively. First a temporal velocity is computed, then a Poisson system is solved for pressure to assure mass conservation based on the temporal velocity. Further the velocity is updated using the new pressure field, lastly the scalar equation is solved based on the updated velocity. The temperature in the source term in the momentum equations and the material properties are taken from the previous time step/inner iteration. To assure a proper coupling between the velocity and temperature fields, i.e. the momentum and energy equations, multiple inner iterations were used. An assessment of the convergence rate deemed two inner iterations sufficient.

The Boussinesq-approximation is a common assumption usually employed in buoyant simulations. The applicability of the Boussinesq approximation requires that the density difference ratio $\Delta\rho/\rho$ should be small. Gray and Giorgini [33] assessed the validity of the Boussinesq-approximation and they concluded that as long as the Rayleigh number $Ra < 10E19$ the Boussinesq-approximation is valid in water. Webb et al. [25] employed the Boussinesq-approximation on a 300°C buoyant jet in air where the above criteria was not met in part of domain, i.e. in close vicinity to the jet orifice. However, although the density difference ratio $\Delta\rho/\rho$ in their case was about 0.5 at the most, they concluded that the results should not be significantly affected, particularly not in the far field. Here the density ratio is 0.01, based on this it is anticipated that the

Boussinesq approximation constitutes a valid assumption in the present case.

The flow associated with an unconfined buoyant plume above a heated horizontal cylinder is inherently different from a buoyant jet which should be taken into account setting up a simulation. For buoyant jets, the mass flow rate is normally prescribed as a boundary condition along with the inlet jet temperature. However, for a buoyant plume rising from a heated cylinder no mass flow is specified, only the cylinder boundary condition is prescribed. Moreover, the computational domain must be chosen accordingly. Jets has a specified inflow and it is therefore natural to choose an outlet boundary condition far downstream. A relatively narrow domain may be chosen if the entrainment is specified, e.g. in terms of the entrainment coefficient α, cf. Morton et al. [34]. Furthermore, the momentum level in a buoyant plume rising from a heated cylinder may be very low compared to a jet. Boundary conditions, sharp mesh transitions and ill-conditioned parameters will influence the buoyant plume significantly. A large computational domain is required to emulate an unconfined cylinder. Preliminary simulations with smaller domains influenced the weak plume significantly. The flow domain was $75D/150D/4D$ width/height/depth with the cylinder located $37.5D$ above the bottom boundary. Considering the set of equations governing incompressible fluids, where any influence from the pressure affects the entire domain instantaneously, care must be taken when choosing boundary conditions.

The cylinder boundary conditions chosen here are taken from an earlier experimental investigation of the buoyant plume above an unconfined heated horizontal cylinder with a Rayleigh number of $9.4E7$ under quiescent conditions, see Grafsrønningen and Jensen [1]. A polynomial $T(\theta) = p_1\theta^4 + p_2\theta^3 + p_3\theta^2 + p_4\theta + p_5 + T_\infty$ where p_n are coefficients fitted to the experimental data and T_∞ is ambient temperature, was specified as the thermal boundary condition, see

p_1	-0.000000029508602
p_2	0.000011218941671
p_3	-0.001040500036804
p_4	0.031687468152510
p_5	21.20760727142974

Table 1: Coefficients for thermal boundary condition polynomial $T(\theta) = p_1\theta^4 + p_2\theta^3 + p_3\theta^2 + p_4\theta + p_5 + T_\infty$. $\theta = 0$ is lower stagnation point, $T_\infty = 20.89^oC$

table 5.

Periodic boundary conditions were specified in all three spatial directions. The large computational domain facilitated such an approach. An area above the cylinder was defined as the area of particular interest, i.e. up to $6D$ above cylinder center. The simulations were run for some time (3 min.) until the initial transients were swept out and a statistical steady state condition was achieved in the area of interest. The required initialization period was determined based on preliminary simulations and confirmed by a a post-simulation assessment of the trend of temporal plume center velocity at different heights above the cylinder. After the initializing period statistics were collected for 150000 time steps which is equivalent to about 70 flow throughs through the area of interest based on the characteristic velocity $U_0 = \sqrt{g\beta\Delta TD}$. Grafsrønningen et al. [2] estimated the frequency of the shedding plume above a horizontal cylinder for Rayleigh numbers $2.05E7$, $4.91E7$, and $7.94E7$. The plume periods were 60-90s for the lowest Rayleigh number and about 30s for the highest Rayleigh number. Hence, the frequency increases for increasing Rayleigh number. It is estimated that a plume period for $Ra = 9.4E7$ is in the order of 20s. Thus 150000 time steps would capture 20-25 plume periods. The plume was far from reaching the upper boundary when the simulation stopped, hence the cylinder was unaffected by the recirculating plume entering from the bottom of the computational domain. Statistical stationary conditions were achieved in the area of interest throughout the statistical period using periodic boundary conditions.

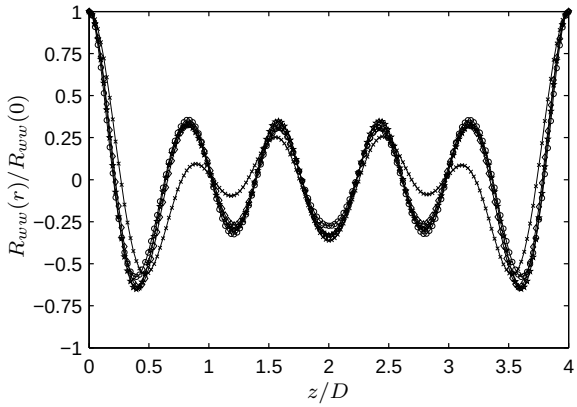

Figure 1: $R_{ww}(r)$ × 100 mm, ⋆ 150 mm, ⋄ 200 mm, and ∘ 250 mm above pipe center.

A domain depth of $4D$ was chosen based on preliminary simulations with smaller domains. Particularly simulations with computational domain depths of $1D$ proved to provide incorrect results since the fluctuating velocity field was correlated through the entire computational domain in the spanwise direction. The normalized two-point correlation (4) for the spanwise velocity fluctuation $w = \tilde{W} - \bar{W}$ in the spanwise direction above the cylinder is shown in Figure 1.

$$R_{ww}(r) = \overline{w(z,t)w(z+r,t)} \tag{4}$$

Here, r denotes the incremental distance in the z-direction. The w-velocity was chosen as the u, and v components are influenced by a shedding motion and require phase-averaging in order to predict the two-point correlation based on turbulent motion only. The two-point correlation (4) in Figure 1 quickly drops below and starts oscillating about zero which suggests that the computational domain is large enough in the spanwise direction.

As mentioned earlier, CDP allows for unstructured grids, an unstructured grid mainly consisting of hexagonal elements was therefore chosen for the simulation. A highly inhomogeneous two-dimensional grid was created in the XY-

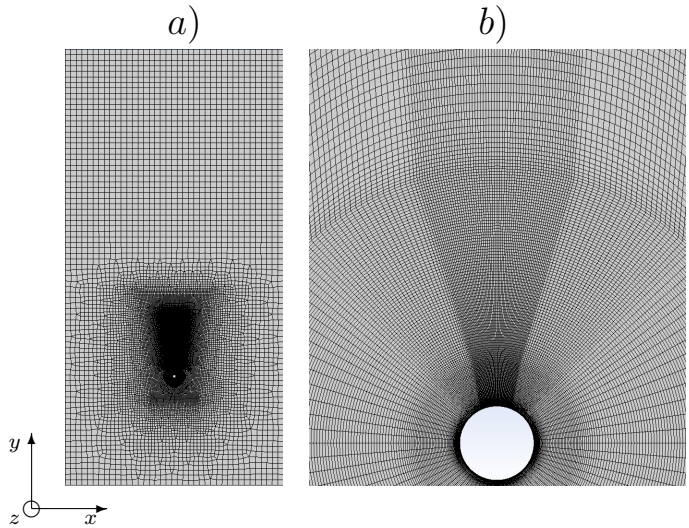

Figure 2: Mesh used in simulation. a) entire domain $4.0m/8.0m/0.216m$ width/height/depth, b) close up view of cylinder. Cylinder diameter is $D = 54mm$, origin in cylinder center.

plane and extruded in the span-wise direction along the cylinder. The plume proved highly sensitive to mesh transitions far downstream the area of interest, hence a fine mesh was used up to 30D downstream the cylinder. The mesh used in the simulations (viewed in a plane) is shown in Figure 2.

The spatial resolution in LES is very important. The grid in a LES should be fine enough to resolve 80% of the energy, thus the residual 20% is modeled, cf. e.g. Pope [23]. The smallest eddies in a turbulent flow is characterized by the Kolmogorov length scale $\eta = (\nu^3/\varepsilon)^{1/4}$. However, in thermal flows with Prandtl number larger than unity the smallest scales are described by another scale, namely the "conduction cut-off", see Batchelor [35]. Batchelor gave an expression for the conduction cut-off similarly to the Kolmogorov length scales, namely $\eta_B = (\nu\alpha^2/\varepsilon)^{1/4}$, hence for $Pr > 1$, $\eta_B < \eta$.

The smallest viscous scale may be expressed as

$$\eta = Gr^{-(3/8)}D \tag{5}$$

where the turbulent dissipation rate is approximated as $\varepsilon = U_0^3/L = (g\beta\Delta TD)^{3/2}/D$.

y $[mm]$	x^+	y^+	z^+	χ^+	ψ^+	ϕ^+
50	4.2	7.5	16.8	11.1	19.8	43.9
75	5.6	12.6	16.8	15.6	32.9	43.9
100	8.0	14.7	16.8	20.8	38.4	43.9
125	10.0	14.7	16.8	26.1	38.4	43.9
150	11.0	14.7	16.8	31.3	38.4	43.9
175	14.0	14.7	16.8	36.5	38.4	43.9
200	14.3	14.7	16.8	37.4	38.4	43.9
225	16.4	21.0	16.8	42.8	54.9	43.9
250	16.9	33.6	16.8	44.1	87.8	43.9

Table 2: Grid size above cylinder. x^+, y^+, z^+ are grid sizes based on η whereas χ^+, ψ^+, and ϕ^+ are computed from η_B

Thus the conduction cut-off scale becomes

$$\eta_B = Gr^{-(3/8)} Pr^{-1/2} D. \tag{6}$$

The wall-normal grid resolution on the cylinder and in the plume area were specified accordingly. A post-simulation assessment of the grid resolution revealed slightly less strict values for η and η_B than equations (5) and (6) yielded. At 90° circumferential angle on the cylinder wall $y^+ = nu^*/\nu = n/\eta = 0.42$ and $t^+ = n/\eta_B = y^+ Pr^{1/2} = 0.97$ where n is wall normal grid length and $u^* = \sqrt{\tau_w/\rho}$ is friction velocity. Table 2 shows the dimensionless length scales based on the viscous and conduction cut-off length scales η and η_B. The grid sizes in all spatial directions are sufficiently small for a well resolved LES. The time step was set to $t^* = tU_0/D = 0.0027$ where t is the physical time step.

3. Results

The results presented herein are the mean and fluctuating components from LES data compared with experimental results from Grafsrønningen and Jensen [1]. For LES, the spatial filtered temporal quantities, i.e. vertical velocity $\tilde{V}$, horizontal velocity $\tilde{U}$, temperature $\tilde{T}$ and pressure $\tilde{P}$, are decomposed into a mean and a fluctuating component, thus $\tilde{V} = \bar{V} + v$ for the vertical velocity. $\bar{V}$

is arithmetic mean of the ensemble

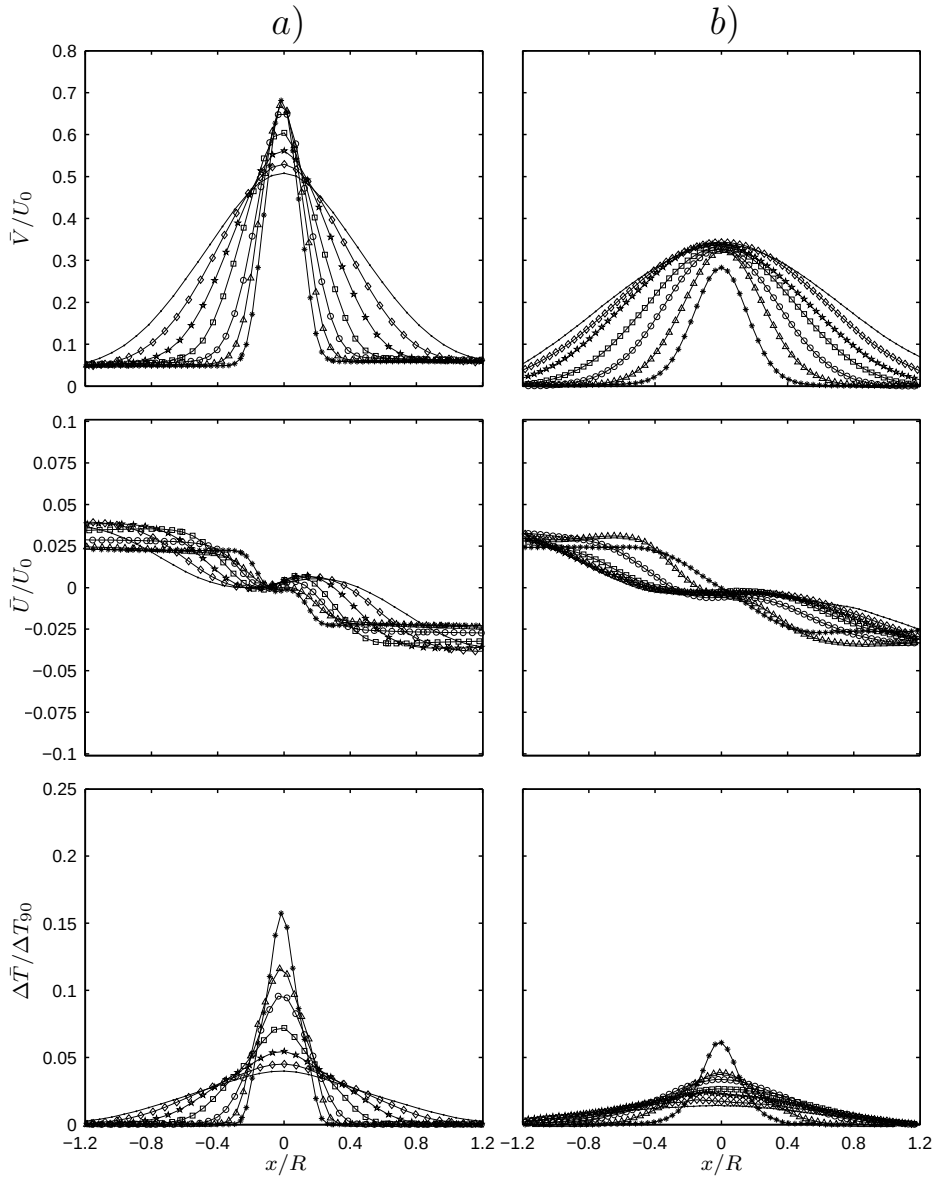

Figure 3: a) LES b) experiments – Vertical velocity $\bar{V}$, horizontal velocity $\bar{U}$, and temperature excess $(\bar{T} - T_\infty)$ $*$ $100mm$, $\triangle$ $125mm$, $\bigcirc$ $150mm$, $\square$ $175mm$, $\star$ $200mm$, $\diamond$ $225mm$, $\cdot$ $250mm$ above cylinder center.

$$\bar{V} = \frac{1}{n}\sum_{i}^{n} \tilde{V}_i \tag{7}$$

where $\tilde{V}_n$ is the vertical velocity. Further, the fluctuating component, here for v, is presented using variance

$$\overline{v^2} = \frac{1}{n}\sum_{i}^{n}(\tilde{V}_i - \bar{V})^2 \tag{8}$$

and co-variance for cross-correlations such as $\overline{uv}$. Statistics for the experimental data were computed correspondingly. However, the measurements does not yield the same filtered quantity $\tilde{V}$ as LES. The experimental data produce spatial and temporal filtered datasets where the resolution is given by the frequency and spatial resolution of the PIV and LIF measurements. The spatial resolution in the PIV measurements were in the same order as the LES, hence eddies of similar size should be measurable in both techniques. Eddies smaller than the computational grid in LES are accounted for in the subgrid models, whereas the effect of eddies smaller than the PIV resolution are averaged out in the experimental data. Furthermore, pseudo-steady state conditions were achieved both experimentally and numerically, i.e. statistical steady state conditions were accomplished during the time of measurements, both for the numerical and physical experiments, thus in a statistical sense, the statistical datasets are directly comparable.

Figure 3 shows the ensemble averaged results from *a*) LES and *b*) experiments. The subfigures show vertical velocity $\bar{V}$, horizontal velocity $\bar{U}$, and temperature excess $\Delta T = \bar{T} - T_\infty$ respectively. Velocity data is normalized using characteristic velocity U_0 whereas temperature is normalized using $\Delta T_{90} = T_{w90} - T_\infty$. The results show that the vertical velocity for LES is overpredicted compared to the experimental results. The vertical mean velocity in the transitional region, i.e. 100-125 mm downstream the cylinder is in particular overpredicted. Although the simulation results approaches the experimental data further downstream, significant differences can still be seen. Another difference

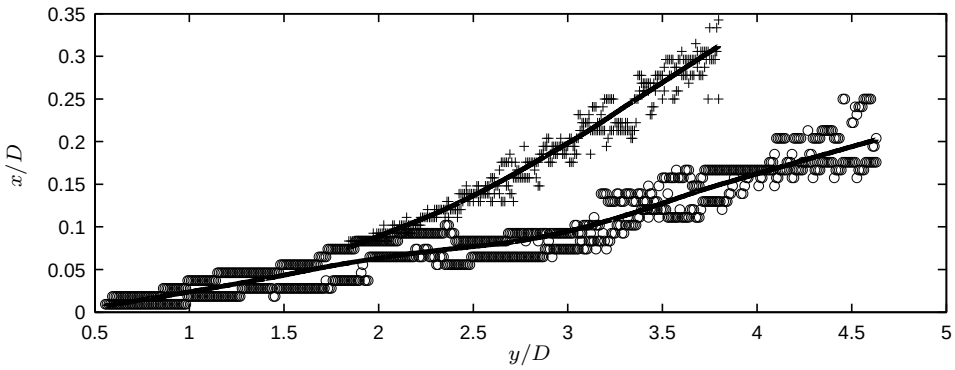

Figure 4: Plume half-width for + experiments and ◯ LES based on location of inflection points for vertical velocity $\bar{V}$. Solid lines are curve fits to the data.

between LES and experimental results worth noting, is the plume widths, the plume predicted by LES is significantly narrower than for the experimental data.

However, water has a large heat capacity C_p, thus the plume temperature excess is small. The reported uncertainty in Grafsrønningen and Jensen [1] ($0.2K$) is relatively large compared to the temperature excess in the plume. Hence, a detailed comparison of temperature excess between the numerical and experimental data may not be fully reliable. Thus, henceforth the plume kinematics is given the most attention when comparing LES data against experimental results. Nonetheless, LES results should provide equally reliable results for all filtered quantities $\tilde{P}$, $\tilde{T}$, $\tilde{U}$, $\tilde{V}$, and $\tilde{W}$.

Figure 4 shows half plume width from LES and experiments in terms of location of the inflection points for the vertical velocity $\bar{V}$. The results clearly show a distinct difference in plume widths downstream the cylinder. At about 1.5 y/D above cylinder center the plume widths are relatively similar. However, further downstream the plume widths for the experimental and LES data deviate significantly. At 3.5 y/D the experimental plume width is about twice that of the LES data.

Figure 5 show velocity correlations $\overline{u^2}$, $\overline{v^2}$, and $\overline{uv}$ and temperature variance

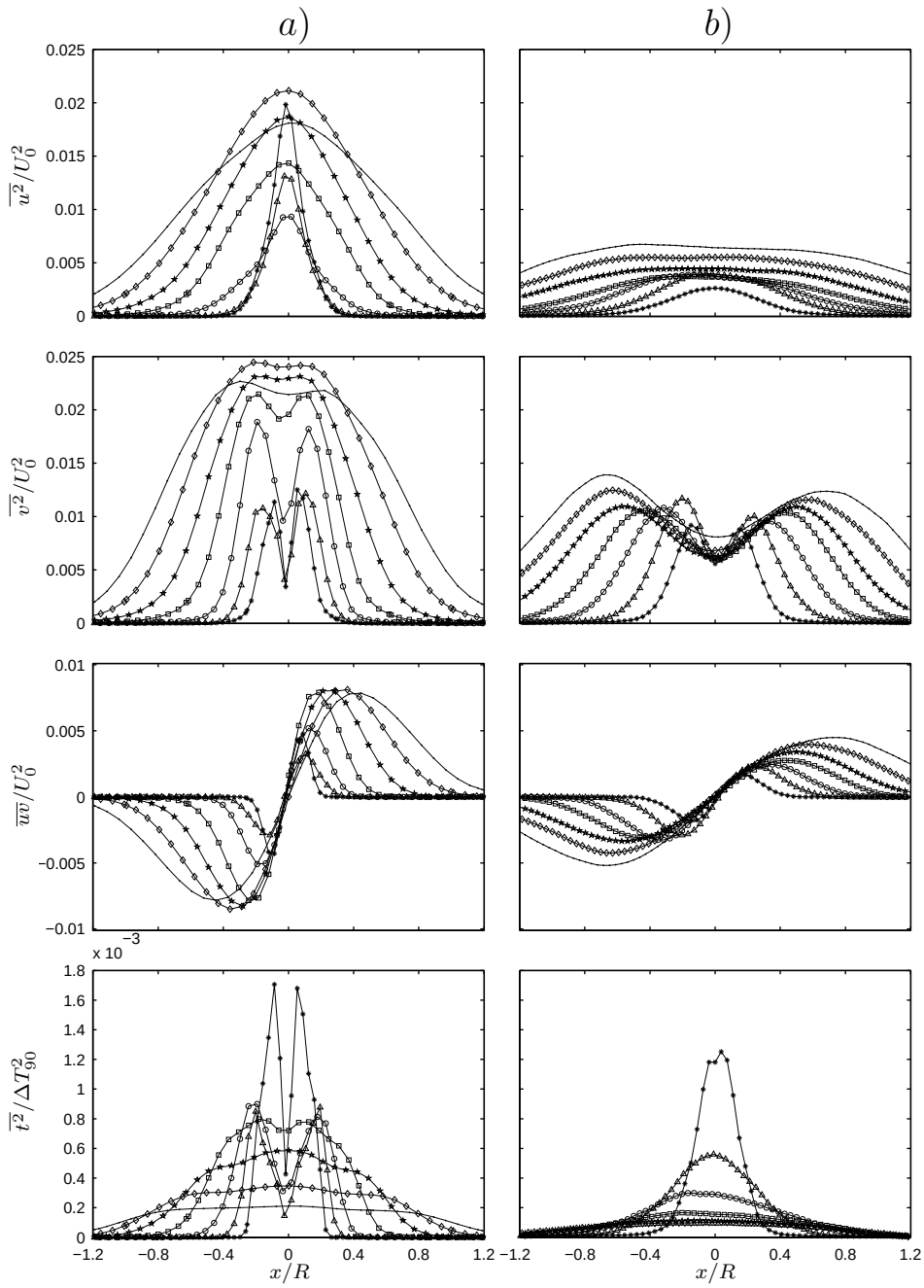

Figure 5: *a*) LES *b*) experiments – Velocity correlations $\overline{u^2}$, $\overline{v^2}$, and $\overline{uv}$, and temperature variance $\overline{t^2}$, $*$ $100mm$, $\triangle$ $125mm$, $\bigcirc$ $150mm$, $\square$ $175mm$, $\star$ $200mm$, $\diamond$ $225mm$, $\cdot$ $250mm$ above cylinder center.

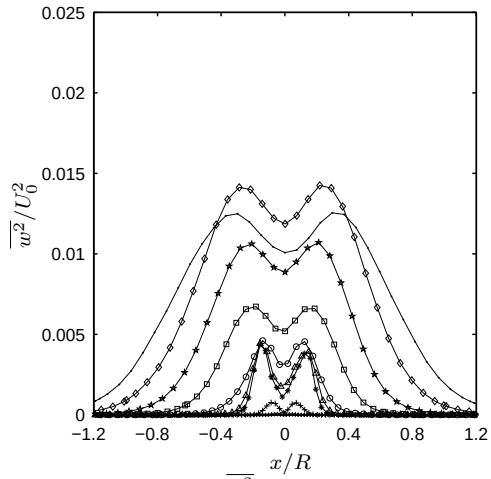

Figure 6: Spanwise velocity correlation $\overline{w^2}$, $\times$ $50mm$, $+$ $75mm$, $*$ $100mm$, $\triangle$ $125mm$, $\bigcirc$ $150mm$, $\square$ $175mm$, $\star$ $200mm$, $\diamond$ $225mm$, $\cdot$ $250mm$ above cylinder center.

$\overline{t^2}$ from a) LES and b) experiments. The velocity variances and velocity cross-correlations in Figure 5 are not necessarily equal to the Reynolds stresses. As briefly mentioned earlier, in buoyant plumes forming above heated horizontal cylinders at intermediate Rayleigh numbers, there may be an appreciable shedding motion similar to vortex shedding downstream cylinders for low Reynolds number cross flow. A decomposition into mean, shedding and turbulent motion is required in order to separate the turbulent effects. However, both the experimental and numerical data were equated in the same way, hence the datasets are directly comparable. The results show that the velocity correlations and temperature variance are similar to the experimental data. However, the magnitude is about twice as large as for the experimental data. Though, the predicted plume width influence the results significantly, the difference in plume width is also clearly distinct when comparing the second order moments.

In Figure 6 the $\overline{w^2}$-component is shown. Since we can assume that large scale shedding mainly takes place in the xy-plane, the influence of the shedding on $\overline{w^2}$ is believed to be very small. This implies that $\overline{w^2}$ should be equal to the spanwise Reynolds normal stresses because $\overline{w^2}$ receives energy only through

redistribution of the other Reynolds stress components. Far downstream, the plume will approach an uniform velocity profile in close vicinity to plume center, i.e. $\partial_x \bar{V} = 0$. Without turbulence production $P = P_k + G_k = -\overline{u_i u_j}\partial_j U_i - g_i \beta \overline{u_i t}$ the turbulence will approach an isotropic state due to redistribution of Reynolds normal stress components $\overline{u^2}$ and $\overline{v^2}$ into $\overline{w^2}$. The spanwise component $\overline{w^2}$ in Figure 6 is as expected smaller than $\overline{u^2}$ and $\overline{v^2}$, but is of same order. This lead us to believe that $\overline{u^2}$ and $\overline{v^2}$, particularly downstream $200mm$ above pipe center for the LES, are mainly due to turbulent effects. In Figure 7 the sum of the velocity correlations across the plume is shown, i.e. for the vertical component $\sum \overline{v^2} = \int \overline{v^2} dx$. The results show that $\overline{u^2}$ and $\overline{v^2}$ starts growing immediately downstream the cylinder. At about 2 y/D $\overline{u^2}$ increases rather rapidly before it decreases from 2 y/D to 2.5 y/D, further downstream it again increases at the same rate as the other components. The spanwise component $\overline{w^2}$ is small compared to the other components until 1.5 y/D. Downstream 2.5 y/D $\overline{w^2}$ increases with roughly the same rate as the other two components. Even further downstream, i.e. $Y/D > 5$ the correlations decrease and approaches each other, yet still $\overline{v^2} > \overline{u^2} > \overline{w^2}$.

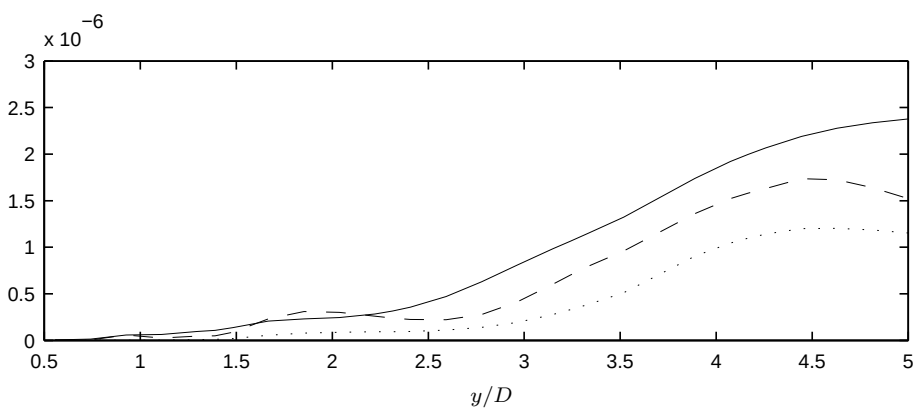

Figure 7: Sum of velocity correlation across plume above cylinder (dashed) $\int \overline{u^2} dx$ (solid) $\int \overline{v^2} dx$ (dotted) $\int \overline{w^2} dx$.

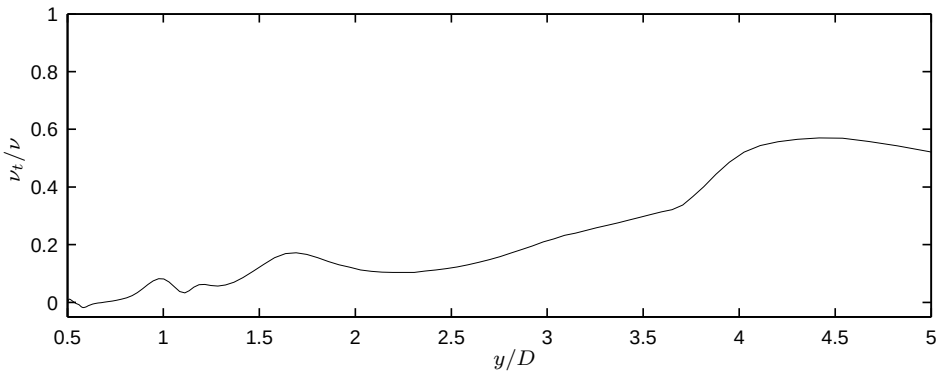

Figure 8: Eddy viscosity ratio ν_t/ν.

The turbulent eddy viscosity ratio ν_t/ν in plume center in Figure 8 show that the contribution from the subgrid model is small. Hence, in terms of contributions from the subgrid model, the simulation is well resolved. The ratio is negative immediately downstream the cylinder, though $-\nu_t/\nu$ is -0.02 at the minimum, further downstream the ratio is positive. In the region of interest ($y/D < 5$), the effect of the subgrid scale model is small, since the absolute value of the turbulent viscosity is less than 0.6 of the kinematic viscosity of water. For comparison, this is the same order of magnitude as the change in molecular viscosity, as a function of temperature, in the same region. The region of negative turbulent viscosity is limited to $y/D < 0.5$ and its absolute value is limited to 0.02 ν, which is significantly less than the variation in molecular viscosity in the same region. Based on these observations, it is unlikely that sub grid model plays an important role in the simulation of the local dynamics of the near-field of the cylinder. This does not mean that significant energy transfer from small to large scale does not occur. It simply means that any such energy transfer should be captured by the present mesh or falls entirely outside the scope of the present sub grid scale model.

Figure 9 shows the vertical velocity normalized against maximum vertical

velocity at the given height for LES and experimental results. Both datasets are self-similar, hence they can be plotted against a nondimensionalized coordinate $\vartheta = \frac{x}{y-B}$, where B is a constant determined from the datasets. See Grafsrønningen et al. [2] for a more detailed description on how ϑ was obtained. (Note that η was used in Grafsrønningen et al. [2] whereas ϑ is used here to avoid confusion with the Kolmogorov length scale η.) Only data from the self-similar region is included, data upstream $175mm$ from the LES is left out, whereas data downstream $250mm$ is not available from the experimental results. The datasets exhibit relative similar characteristics when plotted against ϑ. However, ϑ differ between LES and experimental results, B is $0.1m$ and $0.05m$ for LES and experiments respectively. The Gaussian function $\bar{V}/V_{max} = \exp^{-(D\vartheta)^2}$ is plotted in Figure 9 a) and b) together with the LES and experimental results. D is 8.0 and 7.8 for a) and b) respectively. D is related to the plume growth, i.e. D can be determined from the location of the inflection points $D = 1/\sqrt{2}\vartheta_{inf}$.

For large $|\vartheta|$ the LES results in a) differ from the Gaussian function. A vertical draft velocity of about $1 - 2mm/s$ around the cylinder and plume is predicted by LES which is not observed in the experiments. Further away from the cylinder and plume, i.e. 5-6D from plume center the draft is reduced, yet still present. The use of periodic boundary conditions may cause the observed unphysical draft and may contribute to a slightly reduced shear, thus influencing turbulent production. However, the effect is believed to be small. Furthermore, the vertical velocity is overpredicted in the lower plume region, the plume is narrower than for the experimental data, hence the mean shear is most likely also overestimated. The Richardson number $Ri = Gr/Re^2$ is in the order of $1E4$, hence the effect on the plume should be small. Preliminary simulations with a bounding box were unsuccessful due to large scale vortices forming in the upper part of the computational domain thus influencing the weak buoyant plume.

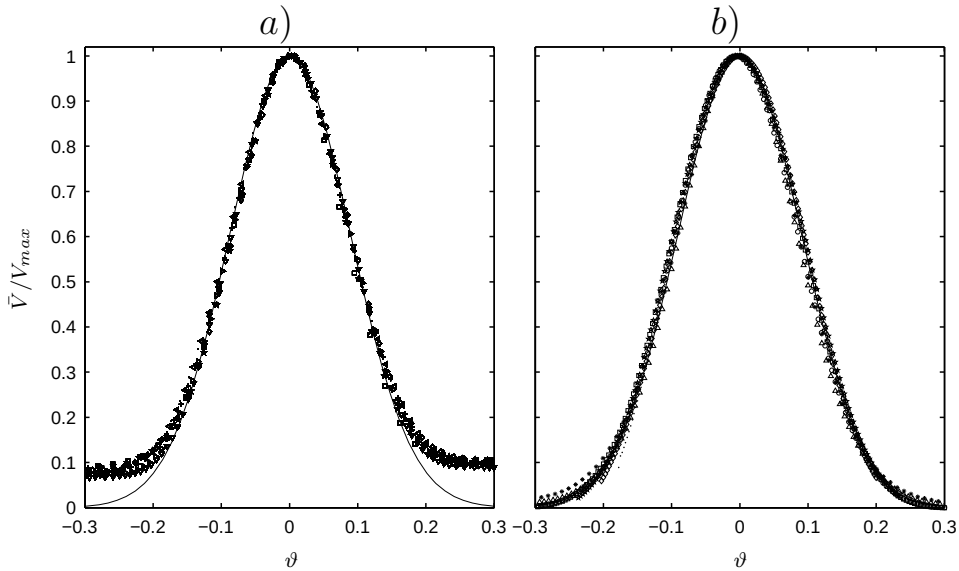

Figure 9: Vertical velocity normalized against maximum velocity at the given height $\bar{V}/V_{max}$ for a) LES and b) experiments [1] for $*$ $100mm$, $\triangle$ $125mm$, $\bigcirc$ $150mm$, $\square$ $175mm$, $\star$ $200mm$, $\diamond$ $225mm$, $\cdot$ $250mm$, $\triangleleft$ $275mm$, $+$ $300mm$, $\triangleright$ $350mm$, and $\triangle$ $400mm$ above cylinder center and the Gaussian expressions (solid line) $\bar{V}/V_{max} = \exp^{-(D\vartheta)^2}$ where $\vartheta = x/(y-B)$. B is $0.1m$ and $0.05m$, and D is 8.0 and 7.8 for a) and b) respectively. Data for $175mm$ to $400mm$ downstream the cylinder is included in a) whereas $100mm$ to $250mm$ is included in b).

Therefore periodic boundary conditions were used in all spatial directions.

The unit length volume flux $F = \int V(x)dx$ for LES and experimental results are shown in Figure 10. LES data are corrected for the synthetic draft to create a sound platform for comparison. The volume flux F compare well, the LES and experimental data exhibit rather similar volume fluxes. Furthermore, for buoyant plumes, in the fully turbulent region, the entrainment is proportional to some characteristic velocity at the same height, see e.g. Gebhart et al. [8]. Thus, due to the constant plume center vertical velocity, the volume flux F should increase linearly. Both datasets are relatively linear, though if carefully examined, the numerical data show sign of a slight s-shaped curvature. The experimental data is practically linear until 3.5 y/D. At $y/D > 3.5$, F is no longer increasing linearly, the rate of increase in F decreases slightly. The plume grew outside the experimental window at this location, thus a reliable F is not

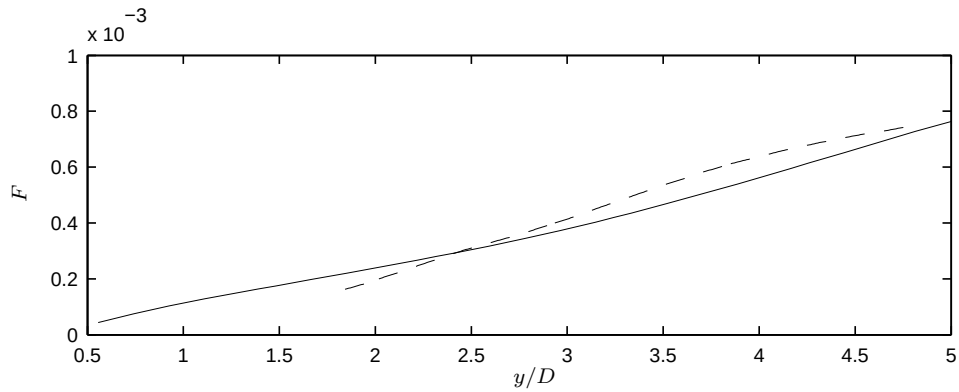

Figure 10: Volume flux per unit length $F = \int V(x)dx$ above cylinder for – LES and −− experiments, corrected for draft velocity.

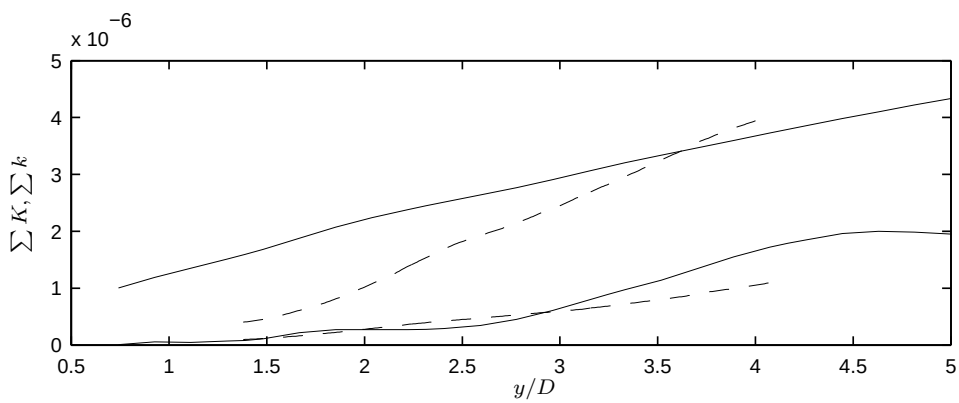

Figure 11: Sum of mean kinetic energy $\sum K = \int 0.5(\bar{U}^2 + \bar{V}^2)dx$ and estimate for fluctuating kinetic energy $\sum k = \int 0.5(\overline{u^2} + \overline{v^2})dx$ across plume. Upper lines show $\sum K$ whereas lower lines show $\sum k$ for – LES and −− experiments.

available downstream $3.5y/D$ from the experimental results.

Kinetic energy in terms of the sum of mean and fluctuating components are shown in Figure 11 for LES and experimental results. The sum of shedding and turbulent effects is here referred to as fluctuating kinetic energy, a decomposition of shedding and turbulent effects are not carried out. Fluctuating kinetic energy is here approximated using streamwise and lateral components only, the spanwise component $\overline{w^2}$ is left out in order to compare LES data directly with experimental results from where only $\overline{u^2}$ and $\overline{v^2}$ are available. The data show that the fluctuating kinetic energy $\sum k$ is rather similar for LES and experiments, whereas the mean kinetic energy $\sum K$ from LES deviate from experimental results, particularly close to the cylinder. The synthetic draft velocity will, to some extent, influence the estimate of mean kinetic energy, particularly in the lower part of the plume.

Buoyant plumes are driven by a energy transfer from potential energy to kinetic energy. As mentioned earlier, water has a large heat capacity compared to e.g. air, thus in buoyant plumes in water the ratio of thermal energy over kinematic energy is large. An estimate of the ratio is $C_p\Delta\bar{T}/K$ which is in the order of $1E7$ in plume center for the LES. The ratio decreases with a factor of about 3 from 2 y/D to 5 y/D.

Turbulent planar buoyant plumes are featured by a temperature excess decay of $\Delta\bar{T} \sim 1/y$, a constant vertical velocity $\bar{V}$ in plume center, and a Gaussian velocity profile see e.g. Gebhart et al. [8] or Rodi [36]. Figure 12 a) shows vertical velocity and b) temperature excess in plume center above the cylinder for the LES data. The dotted line in b) is the theoretical temperature decay in plume center $C/(y-B)$ where $C = 0.12[K/m]$ is a fitted constant and B is as before. The vertical velocity does not become fully constant in plume center, even for large y. Furthermore, the temperature excess $\Delta\bar{T}$ does not fully

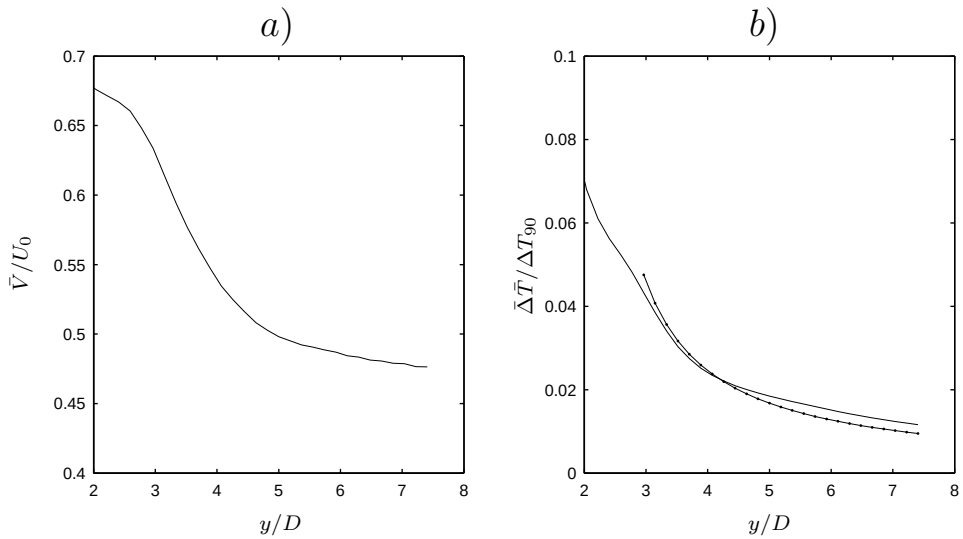

Figure 12: *a*) Plume center vertical velocity $\bar{V}$ and *b*) plume center temperature excess $\Delta\bar{T}$. The dotted line is theoretical (fitted) temperature decay $T \sim 1/y$.

correspond with the expected temperature decay for turbulent buoyant plumes, though the difference is relatively small.

Bastiaans et al. [17] carried out DNS and LES of a transitional plane plume forming above a horizontal heated wire in air in an enclosed cavity. They investigated the performance of several LES sub-grid models and reported that some of the models over-estimated the mean flow with up to 30%, they also reported a striking difference between the DNS and LES results in the transitional region. Similar to Bastiaans et al. [17], Pham et al. [6] reported an over-estimation of the mean velocity of about 11% when using the classical and dynamic Smagorinsky models. A considerable improvement was achieved by using a Lagrangian subgrid-stress model instead of the Smagorinsky models. The averaged and fluctuating quantities matched significantly better. Pham et al. [6] applied different spatial filters to the DNS results to assess the role of turbulence modeling and concluded that there are strong links between different scales in pure thermal buoyant turbulent flow.

Given the relative poor agreement between the LES results and experimental

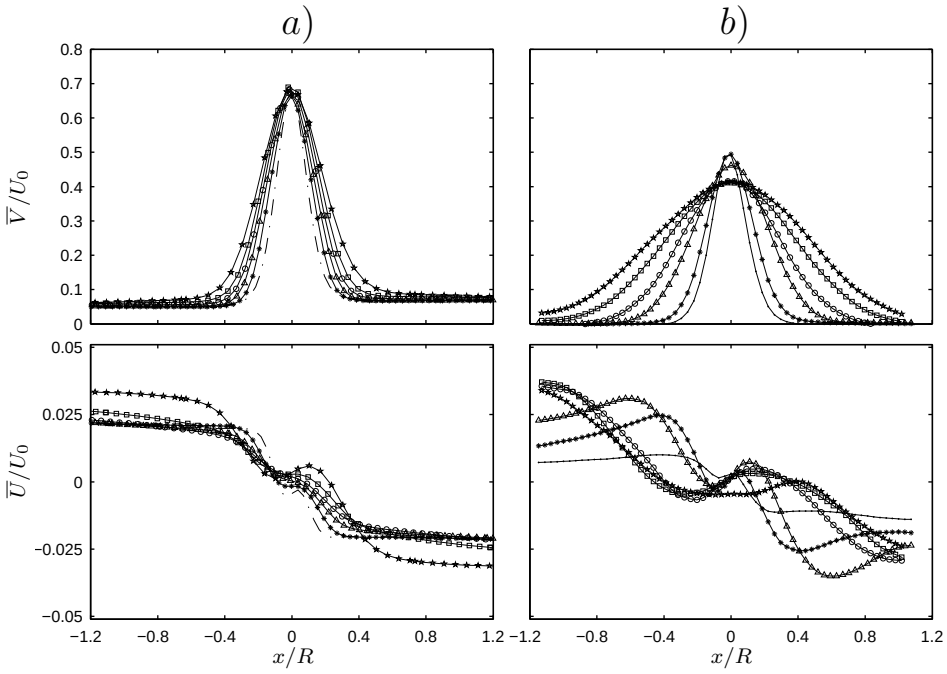

Figure 13: a) LES b) experiments – Vertical velocity V and horizontal velocity U, • 90 mm, $*$ 110mm, △ 130mm, ◯ 150 mm, □ 170 mm, and $\star$ 190 mm above pipe center.

data in Figures 3 and 5, another simulation with a Rayleigh number of $2.05E7$ was carried out and compared against experimental data. The experimental data and boundary conditions were taken from Grafsrønningen et al. [2]. Vertical velocity $\bar{V}$ and horizontal velocity $\bar{U}$ are plotted in Figure 13. The same mesh as described earlier was used, hence the relative resolution was better than in the first simulation. Based on η for the latter simulation, x^+, y^+ and z^+ was 56% of the values in table 2. Similar results are observed here, the predicted plume width is significantly narrower than the experimental data, and the plume center velocities are overpredicted compared to experimental results. Further downstream, i.e. outside the field of particular interest the plume approaches a turbulent state and the plume width increases more rapidly.

Figure 14 show volume visualizations of the LES data. The uppermost subfigures show temperature, the middle subfigures show velocity magnitude

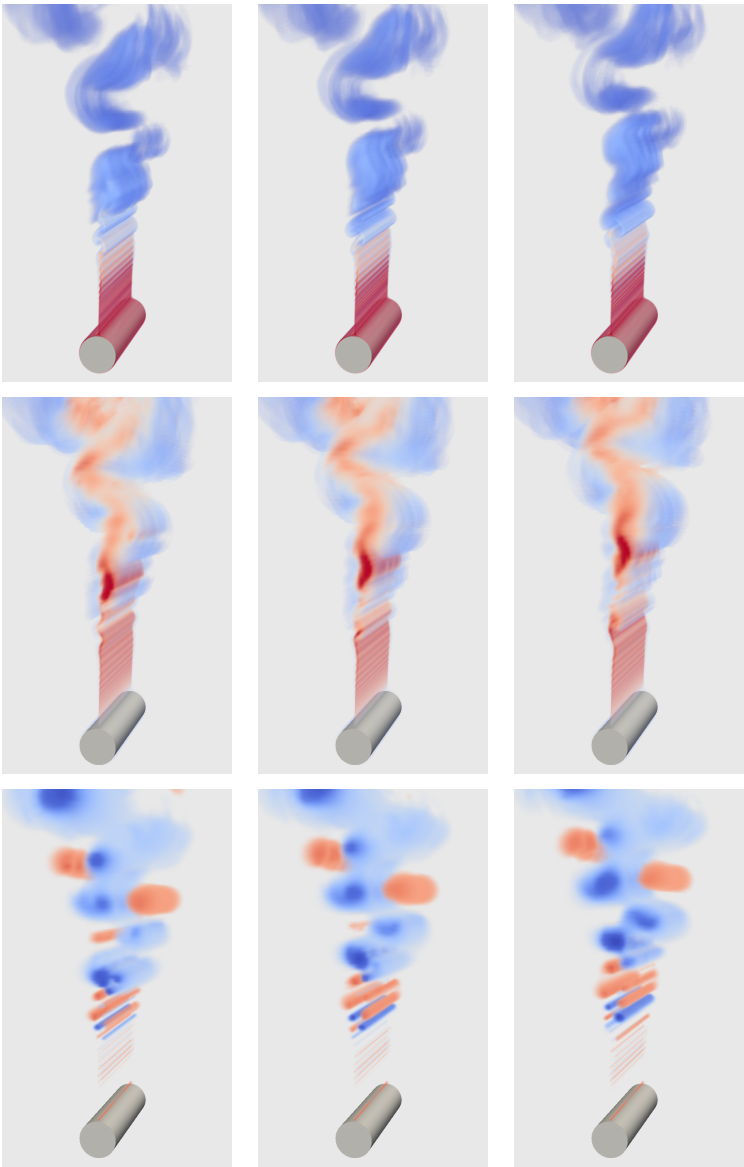

Figure 14: Volume visualization of temperature, velocity and pressure. 1s apart, left to right. See http://tinyurl.com/cxsntun for movie.

whereas the lower show pressure 1 s apart. The plume develops into a three-dimensional flow a distance downstream the cylinder, see movie (http://tinyurl.com/cxsntun) for better spatial and temporal resolution and easier interpretation of the visualization. The volume visualization also show a distinct wavy motion which initiates relatively immediate downstream the cylinder which is convected and amplified downstream. The wavy motion resembles two-dimensional Schlichting-Tollmien waves commonly observed in boundary-layer transition processes, cf. White [37] and Schlichting and Gersten [38].

Figure 15 show the instantaneous horizontal velocity $\tilde{U}$ in the yz-plane. The horizontal velocity clearly exhibit a pattern commonly associated with initial two-dimensional Tollmien-Schlichting waves, see White [37] or Schlichting and Gersten [38] for other examples. According to White [37], for nearly infinitisemal and random perturbations the initial instability in boundary layers will occur as two-dimensional Tollmien-Schlichting waves. Further downstream the two-dimensional waves develop into a three-dimensional a motion. Note that Figure 15 are taken from an another stage in the simulation than the data shown in Figure 14. The point of transition dynamically move up and down above the cylinder, which to some extent is visible in the movie.

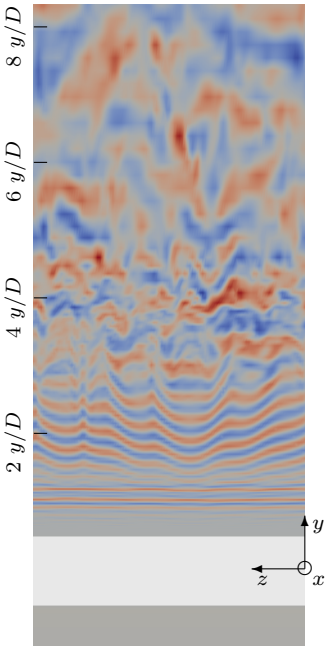

Figure 15: Instantaneous horizontal velocity $\tilde{U}$ in yz-plane above cylinder.

4. Conclusion

Turbulent simulations of natural convection heat transfer from a horizontal cylinder are carried out and compared with experimental data. The results show a considerable difference between the numerical and experimental results. Plume center vertical velocity is highly overpredicted compared to the experimental data, particularly in the lower region the data does not match well, the plume width is also wrongly estimated. The computed half-width about 1.5 y/D downstream the cylinder is comparable to the experimental data, however, 3.5 y/D downstream cylinder, the half-width is about half that of the experimental data. Further downstream the plume resembles the experimental data, though it still suffers from the wrongly computed plume width.

A large number of different setups were tried out to get a better match between the simulations and experimental results. The following parameters were varied in order to try to improve the simulation results:

- Size of domain (width/height/depth)
- Mesh resolution (cylinder wall normal grid length, cylinder circumferential mesh resolution, mesh resolution in plume region, mesh resolution in the cylinder axis direction, and others.)
- Turbulent Prandtl number (0.3 - 0.9)
- Domain boundary conditions (”outlet” - top, ”opening” - top, ”inlet” - bottom, solid walls - top/bottom/left/right, periodic - all)
- Time step length
- Clipping on/off

- Turbulence models (no model, dynamic Smagorinsky, standard Smagorinsky). 95% of the simulations were carried out using the dynamic Smagorinsky as no apparent improvement was seen with the other models

- Variations of the thermal boundary condition (which was taken from the measurements) to assure that a small error in cylinder boundary condition did not influence the results

The LES data exhibit self-similar characteristic downstream 175mm (3.25 y/D) above cylinder center, whereas the experimental data approaches a self-similar state about $125mm$ (2.3 y/D) downstream the cylinder. The LES data exhibit a near Gaussian velocity distribution in the self-similar area, with relatively equal coefficients as for the experimental data. Moreover, constant plume center velocity and plume temperature decay predicted by turbulent similarity solutions, and observed in experiments for turbulent planar buoyant plumes, were not observed in the LES data, though the LES results approached such a state.

The results from the simulation with $Ra = 9.4E7$ indicated that the point of transition initiated at about the same location as in the experiments, but that the plume growth was significantly underpredicted, thus leading to an overestimate for the plume velocities. For the simulation with ($Ra = 2.05E7$) the point of transition is predicted too late, and the velocity data does not match the experimental data very well.

Two-dimensional perturbations similar to Tollmien-Schlichting waves are observed in the LES data ($Ra = 9.4E7$). The perturbations occur relatively immediate downstream the cylinder and are convected and amplified further downstream. Experimental data close to the cylinder is not available, though similar plume widths and a similar fluctuating kinetic energy are observed at about 2 y/D downstream the cylinder. However, further downstream, the results deviate significantly, i.e. the Tollmien-Schlichting like waves continue to

grow in the LES data, whereas the experimental data develops into a fully turbulent flow. Even further downstream, the numerical results develops into a three-dimensional flow, though the results suggest that a fully turbulent state is not reached within the field of particular interest.

Other studies reported in the literature, where the performance of several LES models is scrutinized against DNS data, have concluded that there are strong links between different scales in plumes, particularly in transitional regions, hence interscale and reversed energy transfer is important. DNS and LES results reported in the literature, involving laminar to turbulent transitions in buoyant plumes, suggest that present variants of the Smagorinsky model does not emulate such flows accurately. Reversed energy transfer, i.e. transfer from smaller to larger scales may not be adequately modeled, albeit the eddy viscosity approach allows for this to some extent through negative eddy viscosities. Further, the original Smagorinsky model suffered from excessive dampening in the transitional region due to a constant model coefficient. The dynamic procedure allows for both laminar and turbulent flow, however, it is important that the model is able to accurately determine the state of the flow thus providing appropriate model coefficients. The slow plume growth in the first, and the late transition observed in the latter simulation, may be effects of excessive dampening. The model does not adequately represent the flow state. An assessment of the performance of the turbulence model, other than a qualitative comparison of numerical data against experimental data, was not conducted.

5. Acknowledgments

Financial support for this work was provided by the PETROMAKS project under research grant no. 193215/S60 from the Norwegian Research Council. This work was performed on the Titan Cluster, owned by the University of Oslo and the Norwegian metacenter for High Performance Computing (NOTUR), and

operated by the Research Computing Services group at USIT, the University of Oslo IT-department.http://www.hpc.uio.no/

References

[1] S. Grafsrønningen and A. Jensen. Simultaneous PIV/LIF measurements of a transitional buoyant plume above a horizontal cylinder. *International Journal of Heat and Mass Transfer*, 55:4195–4206, 2012.

[2] S. Grafsrønningen, A. Jensen, and B.A. Pettersson Reif. PIV investigation of buoyant plume from natural convection heat transfer above a horizontal heated cylinder. *International Journal of Heat and Mass Transfer*, 54:4975–4987, 2011.

[3] V.T. Morgan. The overall convective heat transfer from smooth circular cylinders. *Advances in heat transfer*, 11:199–264, 1975.

[4] K. Kitamura, F. Kami-iwa, and T. Misumi. Heat transfer and fluid flow of natural convection around large horizontal cylinders. *International Journal of Heat and Mass Transfer*, 42:4093–4106, 1999.

[5] B.R. Gyles, B. Hægland, T.B. Dahl, A. Sanchis, S. Grafsrønningen, R.B. Schüller, and A. Jensen. Natural convection - subsea cooling; theory, simulations, experiments and design. *Proceedings of the ASME 30th International Conference on Ocean, Offshore and Arctic Engineering*, 2011.

[6] M.V. Pham, F.Plourde, and K.S. Doan. Direct and large-eddy simulations of a pure thermal plume. *Phyics of Fluids*, 19:125103, 2007.

[7] B. Eckhardt. A critical point for turbulence. *Science*, 333:165–166, 2011.

[8] B. Gebhart, Y. Jaluria, R.L. Mahajan, and B. Sammakia. *Buoyancy-induced flows and transport*. Hemisphere Publishing Corporation, 1988.

[9] T.H. Kuehn and R.J. Goldstein. Numerical solution to the navier-stokes equations for laminar natural convection about a horizontal isothermal circular cylinder. *International Journal of Heat and Mass Transfer*, 23:971–979, 1980.

[10] B. Farouk and S.I. Güçeri. Natural convection from a horizontal cylinder - laminar regime. *Transactions of the ASME*, 103:522–527, 1981.

[11] J.H. Merkin and I. Pop. A note on the free convection boundary layer on a horizontal circular cylinder with constant heat flux. *Wärme- und Stoffübertragung*, 22:79–81, 1988.

[12] T. Saitoh, T. Sajiki, and K. Maruhara. Bench mark solution to natural convection heat transfer problem around a horizontal circular cylinder. *International Journal of Heat and Mass Transfer*, 36(5):1251–1259, 1993.

[13] H. Yüncü and A. Batta. Effect of vertical separation distance on laminar natural convective heat transfer over two vertically spaced equitemperature horizontal cylinders. *Applied Scientific Research*, 52:259–277, 1994.

[14] H. Demir. Experimental and numerical studies of natural convection from horizontal concrete cylinder heated with a cylindrical heat source. *International Communications in Heat and Mass Transfer*, 37:422–429, 2010.

[15] K. Noto, K. Teramoto, and T. Nakajima. Spectra and criticla grashof numbers for turbulent transition in a thermal plume. *Journal of Thermophysics and Heat Transfer*, 13:82–90, 1999.

[16] B. Farouk and S.I. Güçeri. Natural convection from a horizontal cylinder - turbulent regime. *Transactions of the ASME*, 104:228–235, 1982.

[17] R.J.M. Bastiaans, C.C.M. Rindt, F.T.M. Nieuwstadt, and A.A. van Steenhoven. Direct and large-eddy simulation of the transition of two-and three-

dimensional plane plumes in a confined enclosure. *International Journal of Heat and Mass Transfer*, 43:2375–2393, 2000.

[18] F. Ham, K. Mattsson, and G. Iaccarino. Accurate and stable finite volume operators for unstructured flow solvers. *Center for Turbulence Research Annual Research Briefs*, 2006.

[19] F. Ham and G. Iaccarino. Energy conservation in collocated discretization schemes on unstructured meshes. *Center for Turbulcence Research - Annual Research Briefs*, pages 3–14, 2004.

[20] F. Ham, K. Mattsson, G. Iaccario, and P. Moi. Towards time-stable and accurate les on unstructured grids. *Center for Turbulcence Research - Annual Research Briefs*, 2005.

[21] C.D. Pierce. *Progress-variable approach for large-eddy simulation of turbulent combustion.* PhD thesis, Stanford University, 2001.

[22] M. Germano, U. Piomelli, P. Moin, and W.H. Cabot. A dynamic subgrid-scale eddy viscosity model. *Phys. Fluids A*, pages 1760–1765, 1991.

[23] Stephen B. Pope. *Turbulent flows.* Camebridge University Press, 2000.

[24] Farah Rashid, Magnus Vartdal, and John Grue. Oscillating cylinder in viscous fluid: calculation of flow patterns and forces. *J Eng Math*, 70:281–295, 2011.

[25] A.T.Webb and N.N.Mansour. Towards les models of jets and plumes. *Center for Turbulcence Research - Annual Research Briefs*, 2000.

[26] J. Worthy. *Large Eddy Simulation of Buoyant Plumes.* PhD thesis, Cranfield University, 2003.

[27] D. You and P. Moin. A dynamic global-coefficient subgrid-scale model for large-eddy simulation of turbulent scalar transport in complex geometries. *Center for Turbulcence Research - Annual Research Briefs*, 2007.

[28] J. Worthy and P. Rubini. A study of LES stress and flux models applied to a buoyant jet. *Numerical Heat Transfer, Part B:Fundamentals: An International Journal of Computation and Methodology*, 48:235–256, 2005.

[29] Z.H. Yan. Large eddy simulations of a turbulent thermal plume. *Heat Mass Transfer*, 43:503–514, 2007.

[30] J.H.Ferziger and Milovan Perić. *Computational Methods for Computational Fluid Mechanics*. Springer-Verlag, 2002.

[31] J. Kim and P. Moin. Application of a fractional time-step method to incompressible Navier-Stokes equations. *Journal of Computational Physics*, 59:308–323, 1985.

[32] K. Mahesh, G. Constantinescu, and P. Moin. A numerical method for large-eddy simulation in complex geometries. *Journal of Computational Physics*, 197:215–240, 2004.

[33] D.D. Gray and A. Giorgini. The validity of the boussinesq approximation for liquids and gases. *International Journal of Heat and Mass Transfer*, 19:545–551, 1976.

[34] B.R. Morton, G. Taylor, and J.S. Turner. Turbulent gravitational convection from maintained and instantaneous sources. *Proceedings of the Royal Society of London. Series A, Mathematical and Physical Sciences*, 234:1–23, 1956.

[35] G.K. Batchelor. Small-scale variation of convected quantities like temper-

ature in turbulent fluid. Part 1. General discussion and the scale of small conductivity. *Journal of Fluid Mechanics*, 5(1):113–133, 1959.

[36] W. Rodi. *Turbulent buoyant jets and plumes.* Pergamon Press, 1982.

[37] F.M.White. *Viscous Fluid Flow.* McGraw-Hill International Editions, 1991.

[38] H. Schlichting and K. Gersten. *Boundary-layer theory.* Springer, 2000.